COMPUTATIONAL APPROACHES TO UNDERSTANDING OXYGEN DIFFUSION IN CANCER GROWTH DYNAMICS

COMPLEXITY72H

Natalia Briñas
Dpt de Matemáticas, Universidad Carlos III de Madrid (GISC)
28911 Leganés, Madrid, Spain.
nbrinas@math.uc3m.es

Emanuelle Capelli
Politecnico di Torino
Université Paris-Saclay
capelli1042@gmail.com

Michele Lambresa
Politecnico di Torino
Université Paris-Cité
michi.lambresa@gmail.com

Hae Seong Lee
Department of Physics
Sungkyunkwan University
Suwon, Republic of Korea
sng1225@skku.edu

Elias Najarro
IT University of Copenhagen
Copenhagen, Denmark
enaj@itu.dk

Om Roy
Department of Computer and Information Sciences
Strathclyde University
Glasgow, United Kingdom
o.roy.2022@uni.strath.ac.uk

Javier Galeano
Complex System Group-UPM - GISC
Universidad Politecnica de Madrid, Spain
javier.galeano@upm.es

Pilar Guerrero
(GISC)
Dpt. de Matemáticas, Universidad Carlos III de Madrid
28911 Leganés, Madrid, Spain.
pilar.guerrero@uc3m.es

June 28, 2024

ABSTRACT

The growth of cancerous cells is governed by a myriad of factors. Notably, oxygen and mechanical forces play a crucial role in governing tissue morphogenesis in general and carcinogenesis in particular. In this work, we explore the role of oxygen diffusion and inter-cellular forces in the growth of cancerous cells embedded in a population healthy cells. We build two complementary morphogenetic diffusion and growth models. Firstly, a vertex model based on a Voronoi tessellation of the cell tissue in which diffusion dynamics are solved with finite element method (FEM). Secondly, a purely diffusive model based on the graph Laplacian where nodes encode oxygen concentration and edges the diffusion coefficients. The models provide a simulation framework to investigate the role of factors such as oxygen distribution, membrane mechanical properties, and noise in the morphogenetic fate of cancerous tissue.

Keywords Cancer disease · oxygen diffusion in cancer growth · complex network · vertex model · finite elements

1 Introduction

Cancer represents a complex system problem characterized by intricate interactions between cancer cells and their surrounding tissue microenvironments ([Rejniak, 2016]). Clinical approaches that exclusively target cancer cells frequently result in unsatisfactory outcomes, including resistance, tissue invasion, and failure of treatment. These issues arise from unexpected behaviors inherent in the dynamic systems of cancer tissues.

Tissue morphogenesis is controlled–among other factors–by the mechanical properties of cells. Cellular processes such as cell division, apoptosis, or changes imposed by the environment on the epithelium can alter the morphogenic dynamics of cells. Understanding the physics of morphogenesis requires taking into account the laws of mechanics, which imply that forces acting in a tissue have to be balanced. The internal and external forces that act to deform the tissue are balanced by friction or viscous forces ([Alt et al., 2017]).

Cells within tissues are interconnected by adhesion molecules along their shared boundaries and exert forces on each other. Mechanical models, such as vertex models, have proven valuable as mathematical tools in biology become increasingly important. These models have been applied to study various phenomena, demonstrating the roles of forces in developmental biology (Alt et al. [2017]) or in cancer cell (Metzcar et al. [2019]). Examples include cell migration in mouse embryos (Trichas et al. [2012]), the Drosophila wing imaginal disc (Kursawe et al. [2015]), and cancer invasion Friedl and Gilmour [2009]. In vertex models, the network of adherens junctions is represented by polygons defined by vertex positions, providing a well-defined structure to accurately capture epithelial tissue behavior.

Traditional approaches describe tissue morphology through the quasi-steady state solution of the Hamiltonian (Nagai and Honda [2001], Drasdo [2000], Farhadifar et al. [2007]). Various energy functions have been proposed, with the function introduced in Farhadifar et al. [2007] gaining extensive use in epithelial modeling. This energy function was incorporated into a two-dimensional model representing one side of the Drosophila wing epithelium cells. The dynamics of tissue dependence on energy function parameters have been classified, identifying regions where the model accurately replicates real tissue behavior. With the extensive study of these models and their parameters, we can apply this knowledge to a vertex model of cancer tissue, which shares characteristics with other similar tissue models.

Chronic hypoxia triggers metabolic changes, fosters the selection of treatment-resistant cancer stem cells, and promotes invasion and angiogenesis (McKeown [2014], Alarcón et al. [2004]). Tumor cells engage in biochemical and biomechanical communication with stromal cells, allowing them to manipulate normal physiological processes (Hanahan and Weinberg [2011]). Mathematical models can simulate environments that offer controlled conditions that enable scientists and clinicians to investigate emergent clinical behaviors stemming from fundamental cellular hypotheses and to evaluate new therapeutic strategies (Guerrero et al. [2016], Macklin [2017]).

In this paper, we employ computational techniques to investigate the role of oxygen diffusion and inter-cellular forces in cancer growth dynamics. We develop two complementary models: a vertex model based on Voronoi tessellation, where diffusion dynamics are solved using the finite element method (FEM), and a graph-based degree-diffusion approach using the graph Laplacian. These models allow us to simulate the diffusion processes and mechanical interactions within cancerous and healthy cell populations, providing insights into the complex mechanisms driving tumor growth and progression.

2 Material and methods

Oxygen diffusion is fundamental in biological systems and crucial for cellular respiration. In the cell cycle, oxygen availability significantly influences cellular processes such as division. Under normal conditions, cells rely on aerobic respiration, but in hypoxia (low oxygen levels), cells activate signaling pathways such as hypoxia-inducible factor 1 (HIF-1) (Park et al. [2021]), which adjusts gene expression to promote survival under low oxygen. Hypoxia can induce cell cycle arrest, allowing adaptation and survival (Ebbesen et al. [2004]). In cancer, oxygen diffusion is critical because tumors often exhibit hypoxic regions due to rapid growth outpacing blood supply. This hypoxic microenvironment promotes tumor aggressiveness, resistance to apoptosis, and metabolic shifts to anaerobic glycolysis (Infantino et al. [2021]). Cancer cells adapt to hypoxia via HIF-1, enhancing angiogenesis to improve oxygen and nutrient supply (Nagao et al. [2019]). Hypoxia also contributes to treatment resistance, reducing radiotherapy effectiveness and making cells less susceptible to chemotherapy (Cho et al. [2013]). Understanding these mechanisms is vital for the development of effective cancer therapies.

2.1 Hexagonal Voronoi diagram

A Voronoi diagram of points subdivides the plane into exactly n cells that cover the partition of the plane that is near each point.

Suppose $P = \{p_1, p_2, \ldots, p_m\}$ is a set of m points in an n-dimensional space. The space can be partitioned into m Voronoi cells, V_i, each containing all the points in $\mathbb{R}^n$ that are closer to p_i than to any other point. Formally, the Voronoi cell V_i associated with point p_i is defined as:

$$V_i = \{x \in \mathbb{R}^n \mid d(x, p_i) \leq d(x, p_j) \text{ for all } j \neq i\}$$

The function $d(x, y)$ gives the distance between its two arguments. Typically, the Euclidean distance (also known as L_2 distance) is used, which is defined as:

$$d(x, y) = \sqrt{\sum_{k=1}^{n} (x_k - y_k)^2}$$

where $x = (x_1, x_2, \ldots, x_n)$ and $y = (y_1, y_2, \ldots, y_n)$ are points in the n-dimensional space.

Delaunay triangulation for a set of points P in the plane is a triangulation $DT(P)$ such that no point in P is inside the circumcircle of any triangle in $DT(P)$. The circumcircle of a triangle is the circle that passes through all three vertices of the triangle. For a set of points in general position (no four points are cocircular), the Delaunay triangulation is unique.

The Delaunay triangulation is also the dual graph of the Voronoi diagram for the same set of points. This means that each vertex of the Voronoi diagram corresponds to a circumcenter of a triangle in the Delaunay triangulation.

Given three points $\mathbf{p}_i = (x_i, y_i)$, $\mathbf{p}_j = (x_j, y_j)$, and $\mathbf{p}_k = (x_k, y_k)$, the circumcircle can be determined by solving the following system of linear equations:

$$\begin{vmatrix} x_i & y_i & x_i^2 + y_i^2 & 1 \\ x_j & y_j & x_j^2 + y_j^2 & 1 \\ x_k & y_k & x_k^2 + y_k^2 & 1 \\ x & y & x^2 + y^2 & 1 \end{vmatrix} = 0$$

The point (x, y) is within the circumcircle if the determinant is positive.

A hexagonal Voronoi diagram is a special case of a Voronoi diagram where each cell is hexagonal. This configuration arises naturally when points are arranged in a hexagonal lattice, which is common in biological tissues.

Biological tissues often exhibit a hexagonal packing of cells due to the efficient packing and structural stability of hexagons. When modeling such tissues, using a hexagonal Voronoi diagram provides a realistic representation of the cell boundaries.

Delaunay triangulation of the points defining the hexagonal Voronoi is then used to provide an efficient way to represent cell connectivity each triangle represents a shared boundary between three cells.The regular structure of the hexagonal grid ensures that the Delaunay triangulation will not have degenerate or skinny triangles, preserving the geometric properties of the tissue.

2.2 Vertex model

In vertex models, cells typically adhere to deterministic equations of motion, with variations among models primarily arising from differences in force definitions. One approach involves explicitly identifying the forces acting on each vertex, such as tension and pressure. Another method considers forces generated from energy minimization, where the energy function represents the total stored energy in the cells' body and membrane. This energy function, dependent on vertex positions, corresponds to the work required to deform the cell junction network.

To describe the dynamics of the characteristic polygonal morphology in a planar vertex model, the forces generated by a specified energy potential can be translated into an equation of motion for the N vertices that represent the tissue, denoted as $\mathbf{r} = \{r_i \mid r_i \in \mathbb{R}^2, i = 1, \ldots, N\}$. Each vertex's dynamics can be modeled by a deterministic overdamped equation of motion Drasdo [2000], where inertial terms are negligible compared to dissipative terms, and the viscosity parameter γ is consistent for each vertex in the system:

$$\gamma \frac{\mathrm{d}r_i}{\mathrm{d}t} = F_i(\mathbf{r}),$$

where $F_i(t)$ represents the total force acting on vertex i at time t, derived from the energy potential E as $F_i = -\nabla_i E$. The chosen energy potential encapsulates the biophysical properties of the cells relevant to the tissue under study and typically takes the form Farhadifar et al. [2007]:

$$E(\mathbf{r}) = \sum_{\alpha} \left[\frac{K_\alpha}{2}(A_\alpha - A_\alpha^0(t))^2 + \frac{\Gamma_\alpha}{2} L_\alpha^2 \right] + \sum_{\langle ij \rangle} \Lambda_{ij} l_{ij},$$

where the first summation covers all cells α in the tissue, incorporating cell-intrinsic energy terms related to elasticity and contractility. Elasticity is described by deviations from a preferred area $A_\alpha^0(t)$, modulated by an elasticity constant K_α. Similarly, cell contractility is introduced through an elastic term dependent on the cell's perimeter L_α and a contractility constant Γ_α. The second summation in the equation accounts for cell interaction terms, such as cell-cell adhesion energy, with Λ_{ij} being a positive constant representing line tension. More complex expressions for the potential can include additional effects like inhomogeneities in contractile tension or non-harmonic energy terms.

2.2.1 Including topological changes

When cellular rearrangements take place, some nodes in the mesh can appear or disappear. We will account for this by introducing a temporary mesh to include estimates of the concentration at the new nodes.

Cell division Cell division is regulated by several different factors, either external, such as chemical stimuli, growth factors and hormones, or internal, like cell cycle regulators. Oxygen concentration plays a crucial role in cellular metabolism and energy production, so therefore, also in cell division. Under normal conditions, healthy cells divide at a controlled rate, ensuring proper growth and tissue maintenance. However, one of the main characteristics of cancer cells often exhibit rapid and uncontrolled division, even under hypoxia when oxygen concentration is very low, which contributes to cancer progression and metastasis. This behavior is due to cancer cells' ability to adapt their metabolism to thrive in low-oxygen environments, often through the activation of hypoxia-inducible factors (HIFs). To represent this in a computational framework we have introduced oxygen dependent division to the vertex model. By setting a threshold for cell division based on intracellular oxygen levels, we can mimic the differential division rates observed in healthy versus cancerous tissues and how these two populations compete in the same tissue. This threshold ensures that only cells with sufficient oxygen levels proceed to divide, thereby providing a more accurate representation of the physiological conditions influencing cell proliferation and the distinct behaviors of healthy and cancerous cells.

When a cell divides, four new nodes are created and the centre of the old cell is removed. The two new cells are of the same type as the parent cell, i.e. if a cancer cell divides the two new cancer cells will be cancerous as well and viceversa. Also, each cell inherits half of the original cell's oxygen concentration. When there is not enough oxygen, cells stop dividing but they still undergo mechanical properties and growing behaviour. The pipeline of this process can be found in Smith et al. [2012].

For this work, we have set a random number of cancer cells in a tissue of 100 cells. We consider the oxygen concentration to be in a range from 0 to 1. For cancer cells the division threshold will be 0.1 meanwhile for healthy cells it will be 0.8. The initial oxygen condition is the same for all cells and it is not updated at each iteration, so once a cell is under the division threshold, it will no divide again. Figure 2 shows how cell division is computed in the vertex model and the tissue evolution based on the oxygen dependent cell divisions.

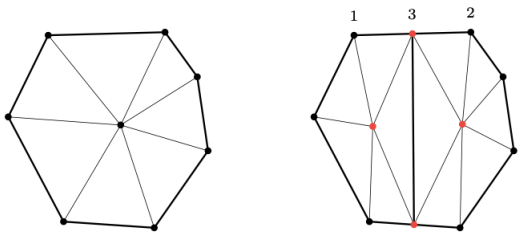

Figure 1: The mesh before cell division and the changes as the result of cell division. The centroid of the mother cell is removed and two new centroids are added to the mesh. The new nodes are in red.

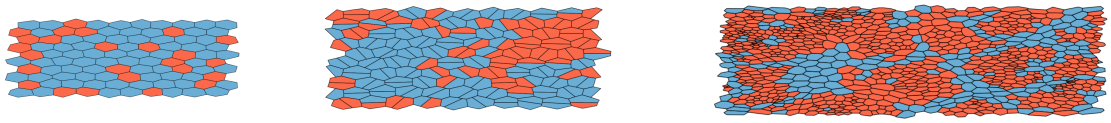

Figure 2: Evolution of the cellular mesh during time. First, the plot shows initial conditions. Healthy cells are represented in blue and cancer cells in red. The second plot represents the second time step, where cells have already divided. The last image shows how cancer cells have divided faster than healthy cells, contributing to cancer spread and grow. Mechanical forces can also be observed at the different cell shapes and location of the cells at each time step.

Two of the new nodes are midpoints of an edge. We can use interpolation to calculate their values. Let c_i denote the concentration at node i. For node 3 in Figure 1, we have

$$c_3 = \frac{1}{2}(c_1 + c_2) \tag{1}$$

and the equation for the other node is analogous.

The other new nodes are centroids of the daughter cells and to approximate the concentration for the new centroids we introduce a temporary mesh. We want to guarantee that the sum of concentration in the daughter cells will be the same as in the mother cell.

The total concentration $C_\alpha(t)$ in cell α can be found by integrating the FE approximation to $c(x,t)$ over the cell. Let L_α be the number of nodes in cell α. Then

Thus, if the total concentration in each of the two daughter cells is known, the value at the new central node can be found. By using the approximation 1, we know the concentrations at all nodes in the new cells, except one. To approximate the total concentration in each cell, we will divide the oxygen concentration in each of the new cells. In the temporary mesh, two of the new nodes are included, but not the centroid nodes. We will also use a node on the new edge. Notice that the new edge will not pass through the centroid of the cell. Instead, for the temporary mesh, we will use the midpoint on the new edge. This point will not be far in distance from the centroid, and we can use the interpolation 1. Thereafter, we can determine the total concentration in each of the new cells.

T1 transitions T1 transitions take place when the distance between two vertices is very small, i.e. is smaller than 3% of the average edge length. Therefore, the concentration at these vertices will nearly be equal, and so we can approximate the concentration at the new nodes to be equal, that is the average of the concentration of the two old nodes. Hence,

$$c_3 = c_4 = \frac{1}{2}(c_1 + c_2) \tag{2}$$

In our model, when a T1 transition occurs, the two nodes after the transition have the same number as before. Thus, a slightly simpler approximation is to let the nodes have the same concentration after a T1 transition as they did previously. We will do this for now, as it will make it simpler to account for the fact that the T1 transition might result in cell death, and a removal of a node.

Cell death Before a cell dies, it shrinks and becomes very small. The concentrations at the nodes in the dying cell, both at the cell boundary and the centroid, will be very similar, and the total concentration in the cell will also be small because its area is small. Hence, if we simply remove the dying cell and the appropriate nodes, we can assume that cell death has negligible effect on the solution.

2.3 Theoretical Framework for Finite Elements and Diffusion Equation with a Reaction Term

We will now present the model that will describe the diffusion of the concentration of the oxygen within the tissue, assuming that a constant flux of oxygen is entering the tissue from the boundaries. This will be useful because the growth and the division of the cells is dependent on the amount of oxygen of which they dispose. The phenomenon of diffusion of oxygen is modeled here with the usual transport equation with a reaction term which describes the consuption of oxygen by the cells during time. The Finite Element Method (FEM) is a numerical tool which is useful to

get the solution of a partial differential equation on a defined, discretized domain. Assuming the discretization of the domain has already been done here, we just introduce the general theory of FEM for the case of transport equation.

The diffusion equation with a reaction term is given by:

$$\frac{\partial u}{\partial t} = D\nabla^2 u + f - \beta u$$

where:

- u is the unknown function (e.g., temperature, concentration).
- D is the diffusion coefficient.
- f is a source term.
- β is the reaction rate coefficient.

Weak Formulation

1. Strong Form to Weak Form

The starting point is the strong form of the PDE. To derive the weak form, we multiply the PDE by a test function v and integrate over the domain Ω:

$$\int_\Omega v\frac{\partial u}{\partial t}\, d\Omega = \int_\Omega v(D\nabla^2 u + f - \beta u)\, d\Omega$$

2. Integration by Parts

Applying integration by parts to the term involving $\nabla^2 u$ reduces the order of the derivative on u. For this, we use the divergence theorem:

$$\int_\Omega v\nabla^2 u\, d\Omega = \int_\Omega \nabla\cdot(v\nabla u)\, d\Omega - \int_\Omega \nabla v\cdot\nabla u\, d\Omega$$

The first term on the right-hand side can be transformed into a boundary integral using the divergence theorem:

$$\int_\Omega \nabla\cdot(v\nabla u)\, d\Omega = \int_{\partial\Omega} v\nabla u\cdot\mathbf{n}\, d\Gamma$$

Here, $\partial\Omega$ is the boundary of Ω and $\mathbf{n}$ is the outward normal vector on the boundary.

3. Applying Boundary Conditions

Let's consider homogeneous Dirichlet boundary conditions ($u = 0$ on $\partial\Omega$) for simplicity. The boundary integral vanishes, leading to:

$$\int_\Omega v\frac{\partial u}{\partial t}\, d\Omega + D\int_\Omega \nabla v\cdot\nabla u\, d\Omega = \int_\Omega vf\, d\Omega - \int_\Omega v\beta u\, d\Omega$$

This is the weak form of the diffusion equation with a reaction term.

Discretization

1. Finite Element Space

Approximate the solution u and the test function v using finite element basis functions. Let $\{\phi_i\}$ be a set of basis functions. We write:

$$u \approx \sum_j U_j\phi_j, \quad v \approx \phi_i$$

2. Galerkin Method

Substitute these approximations into the weak form. The weak form becomes:

$$\sum_j \left(\int_\Omega \phi_i\phi_j\, d\Omega\right)\frac{dU_j}{dt} + D\sum_j\left(\int_\Omega \nabla\phi_i\cdot\nabla\phi_j\, d\Omega\right)U_j = \int_\Omega \phi_i f\, d\Omega - \beta\sum_j\left(\int_\Omega \phi_i\phi_j\, d\Omega\right)U_j$$

3. Matrix Form

Define the mass matrix, M, the stiffness matrix K, the reaction matrix R, and the load vector F:

$$M_{ij} = \int_\Omega \phi_i \phi_j \, d\Omega$$

$$K_{ij} = \int_\Omega \nabla\phi_i \cdot \nabla\phi_j \, d\Omega$$

$$R_{ij} = \beta \int_\Omega \phi_i \phi_j \, d\Omega$$

$$F_i = \int_\Omega \phi_i f \, d\Omega$$

The system of ordinary differential equations is:

$$M\frac{d\mathbf{U}}{dt} + DK\mathbf{U} + R\mathbf{U} = \mathbf{F}$$

Here, $\mathbf{U}$ is the vector of unknown coefficients U_j.

Time Discretization

To solve the system of ODEs, time discretization methods like the backward Euler method, Crank-Nicolson method, or other time-stepping schemes can be employed.

For example, using the backward Euler method:

$$M\frac{\mathbf{U}^{n+1} - \mathbf{U}^n}{\Delta t} + DK\mathbf{U}^{n+1} + R\mathbf{U}^{n+1} = \mathbf{F}^{n+1}$$

Rearranging:

$$(M + \Delta t DK + \Delta t R)\,\mathbf{U}^{n+1} = M\mathbf{U}^n + \Delta t \mathbf{F}^{n+1}$$

2.3.1 FEM and the vertex model

In our model we want to construct the discretized grid for the FEM by triangulating the Voronoi diagram obtained for the cells with the vertex model. We use the Delaunay method in order to triangulate the diagram (fig. 3). Once performed the triangulation we make the simulation of diffusion start with the obtained triangulated grid for the FEM.

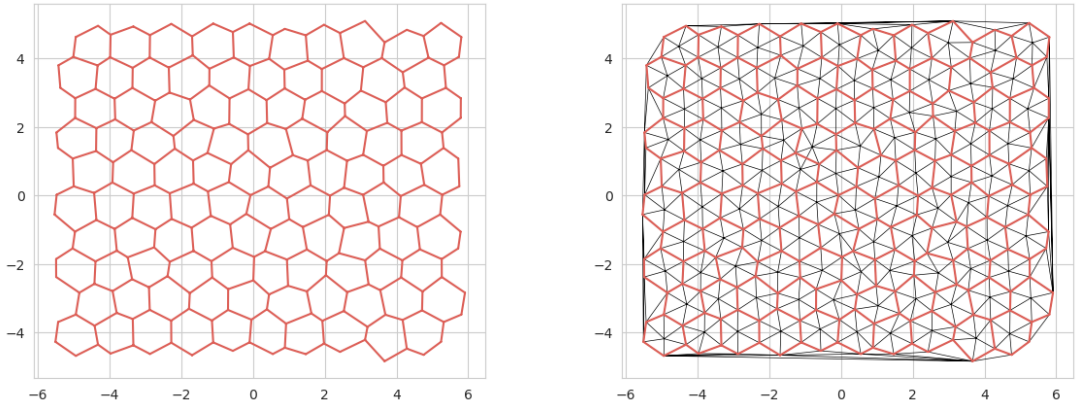

Figure 3: Voronoi diagram of the cells in the tissue and triangulation of the Voronoi diagram for the FEM

If we perform the simulation on this domain with a constant value of the derivative of the function representing the concentration of oxygen at the boundaries ($\nabla u = g$ at the boundaries) and the following values of the parameters:

1. $D = 0.5$

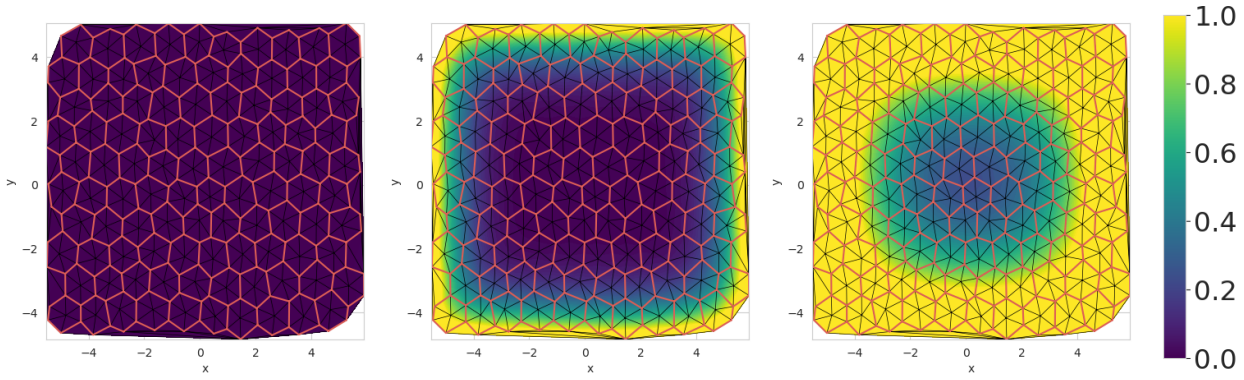

Figure 4: Diffusion of the oxygen in the tissue described by FEM

2. $\beta = 0.01$
3. $g = 10$

we get the following results:

Fig. 4 shows tree snapshots of the oxygen diffusion through the tissue. Boundary conditions impose a constant incoming flux of oxygen from all over the border.
After we have performed the simulation of the diffusion of the oxygen over all the finite element grid, we compute the average concentration of oxygen in each cell, so that it will be available when we will perform the evolution step for the cell division. To do this we just take the average value of the concentration u on the center of the cell and on its vertices.

2.4 Complex Networks as a medium to study Oxygen Diffusion in Cancer Cells

2.4.1 The Diffusion Partial Differential Equation Translated to the Graph Domain

From the Delaunay triangulation, we extract the edges. Each triangle in the triangulation contributes three edges. These edges represent the connectivity between the cell centers. Using the extracted edges, we create an undirected graph where each node represents a cell center, and each edge represents a connection between adjacent cell centers.

To simulate diffusion processes on the graph representing the hexagonal Voronoi diagram, we utilize the Laplacian matrix L derived from the graph's adjacency matrix A.

The diffusion equation in a continuous domain is given by:

$$\frac{\partial u(\mathbf{x}, t)}{\partial t} = D\nabla^2 u(\mathbf{x}, t)$$

where $u(\mathbf{x}, t)$ represents the concentration of the diffusing substance, D is the diffusion coefficient and ∇^2 is the standard Laplace operator.

In the graph domain, the diffusion equation is represented using the graph Laplacian L:

$$\frac{d\mathbf{u}(t)}{dt} = -DL\mathbf{u}(t)$$

where $\mathbf{u}(t)$ is the vector of concentrations at time t, D is a constant representing the diffusion coefficient.

To integrate the diffusion equation over time, we use Euler's method:

$$\mathbf{u}(t + \Delta t) = \mathbf{u}(t) - \Delta t(DL\mathbf{u}(t))$$

where Δt is the time step size, $\mathbf{u}(t)$ is the concentration vector at time t, and $DL\mathbf{u}(t)$ represents the diffusion process as dictated by the Laplacian matrix.

The above equation describes the diffusion of concentration between nodes in a complex network. However, there can be other factors affecting the concentration level as well. For example, the blood vessels can provide oxygen to its neighboring cells. Assume that a blood vessel supplies oxygen to a cell l at a constant rate. Then there should be a

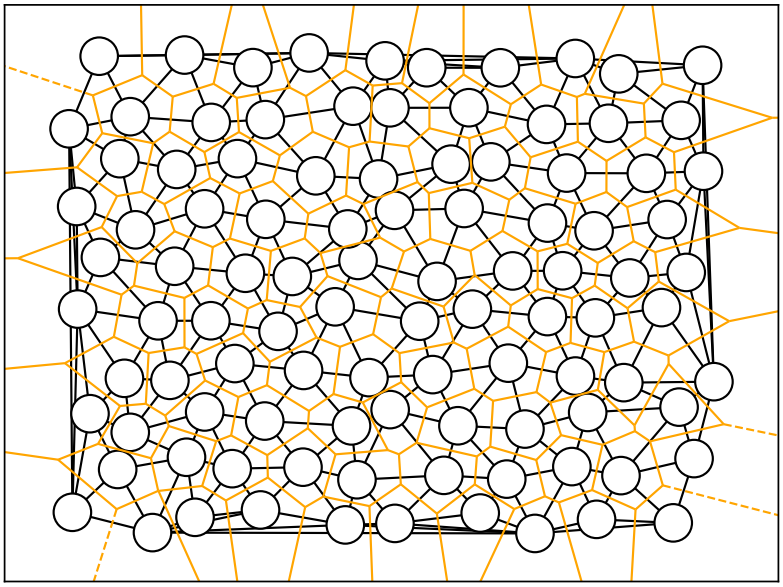

Figure 5: An example of a resulting network with its original voronoi cells. Orange line describes the boundary of voronoi cells which represent cells in a tissue. White circles are nodes in a resulting network which are located at the centroid of each voronoi cells. As oxygen will diffuse through cell walls, the edges are drawn between two voronoi cells when two cells share their boundaries. We note that there are some edges at the boundary of the system that violates this standard. However, this does not affect the oxygen diffusion dynamics because we set the boundary condition that the oxygen concentration is zero at nodes in the boundary of the system.

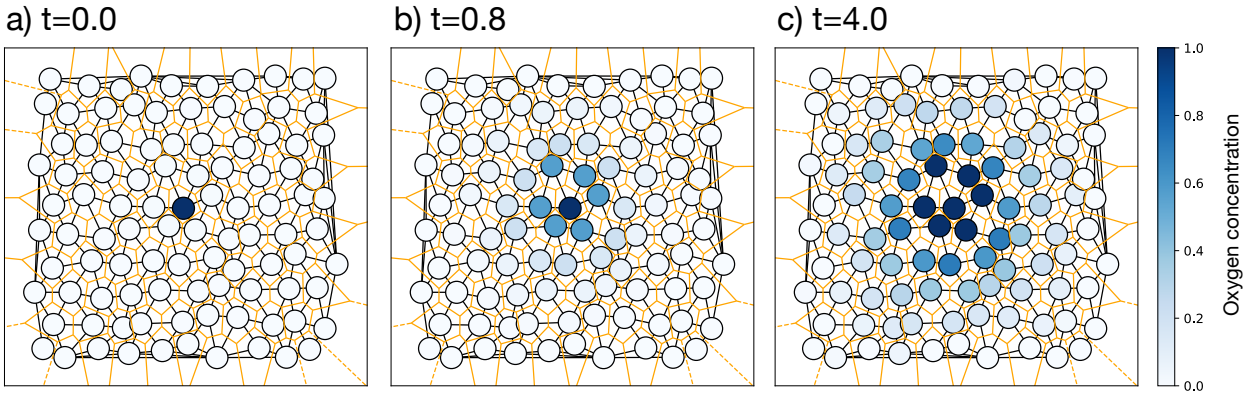

Figure 6: The diffusion of oxygen between nodes with source at the center. The color of each node denotes the oxygen concentration. Initially, oxygen concentration of all nodes are zero except for the source node. The initial concentration of the source node is 1. As a simulation progresses, oxygen in the center spreads out toward the system boundary.

constant term for cell l which describes the constant introduction of oxygen to the cell at a rate k. The equation should be modified as

$$\frac{du_i(t)}{dt} = -D\sum_j L_{ij}u_j(t) + k\delta_{il}.$$

In its vector form, the above equation should be written as below

$$\frac{d\mathbf{u}(t)}{dt} = -DL\mathbf{u}(t) + \mathbf{k}_1,$$

where $(\mathbf{k_1})_i = k\delta_{il}$ is a vector whose elements are all zeros except for lth element, which has a value of k.

The other factors affecting the oxygen concentration in a node is the consumption of oxygen in the cell. Unlike the case in the oxygen influx, the oxygen concentration will decrease as a result of oxygen consumption. In this case, we can assume that a cell uses its oxygen at a constant rate m. Since each cell uses their oxygen, the diffusion equation incorporating oxygen influx and consumption will be

$$\frac{du_i(t)}{dt} = -D\sum_j L_{ij}u_j(t) + k\delta_{il} - m,$$

considering both the oxygen influx rate k for a cell and oxygen consumption rate m for all nodes. In its vector form, the above equation should be written as

$$\frac{d\mathbf{u}(t)}{dt} = -DL\mathbf{u}(t) + \mathbf{k}_1',$$

where the effect of influx and consumption are well incorporated in a single vector $(\mathbf{k}_1')_i = k\delta_{il} - m$. In this example, node l is the only source in the system. Similar to the diffusion-only case, the equation can be integrated by Euler's method as

$$\mathbf{u}(t+\Delta t) = \mathbf{u}(t) + \Delta t(-DL\mathbf{u}(t) + \mathbf{k}_1').$$

However, in this study, we will focus on the case where there is no consumption of oxygen in a cell, and only one source exists.

When the cancer cell is introduced in the system, the diffusion coefficient between cells could be different according to the types of the cells. In a case where a system has heterogeneous diffusion coefficient for each node pairs, the dynamics of a state vector $\mathbf{u}$ will become

$$\frac{du_i(t)}{dt} = -\sum_j D_{ij}L_{ij}u_j(t) + k\delta_{il} \tag{3}$$

$$= -\sum_j L'_{ij}u_j(t) + k\delta_{il}, \tag{4}$$

where $L'_{ij} = D_{ij}L_{ij}$ is the effective laplacian matrix in the system. Therefore, even in this case, the simulation can be conducted as in the case of an identical diffusion coefficient.

Although estimating the diffusion coefficient matrix D_{ij} depends on many biological and environment conditions, we will assume a general case. In many systems it is known that an edge weight between a node i and j depends on the degrees of both nodes. More specifically, the edge weight is proportional to $(k_ik_j)^\theta$ where k_i is a degree of a node i and θ is exponent controlling the sensitivity of edge weight on degrees.

in the case of cancer cells, we use the diffusion coefficient matrix

$$D_{ij} = \begin{cases} D'(k_ik_j)^{\theta_{cancer}} & \text{if at least one of i and j is a cancer cell} \\ D'(k_ik_j)^{\theta_{normal}} & \text{otherwise.} \end{cases} \tag{5}$$

We note that D' is an overall diffusion coefficient that controls the systematic scale of diffusion coefficients and k_i, k_j are degrees of node i and j. Two exponents θ_{normal} and θ_{cancer} determines the difference in diffusion coefficient.

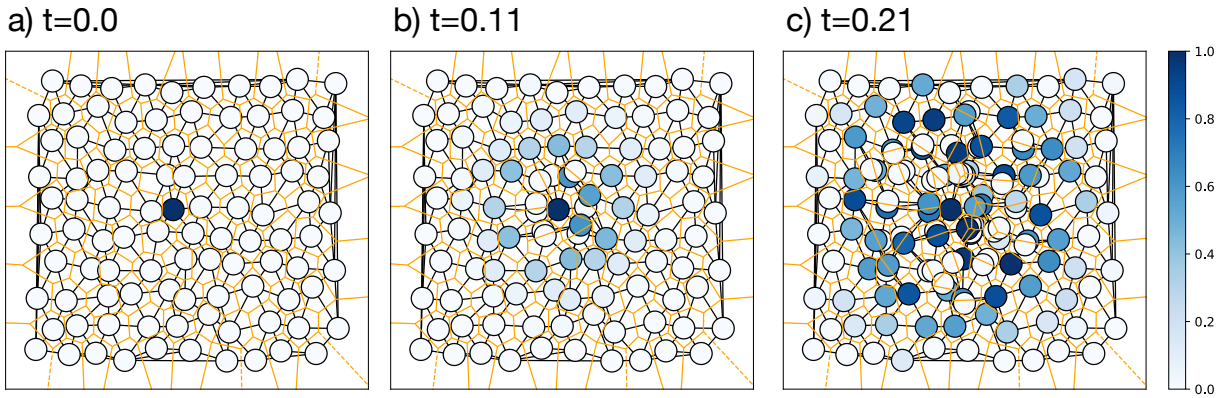

Figure 7: During the diffusion, a cell can be divided into two cells when the oxygen concentration exceeds some threshold value. New cells could become cancer cells with a given probability $p = 0.2$.

2.4.2 Cell division implemented in the graph domain

In addition to the method introduced in the previous section, the cell division is implemented in our complex network approach in a simple way. As a transport network of oxygen is extracted from voronoi diagram, we directly divide a voronoi cell and extract the network again.

When a cell is divided, the network should be updated because the number of cells and their interaction structure changes. The network is updated in the following steps. First, a center point of a cell to be divided is copied and the original point and the copied point are moved away from each other by a constant δ. Then a new voronoi diagram are estimated from the group of center points, and we can get a network with new voronoi diagram.

Motivated by biological facts, the cell division occurs when oxygen concentration exceeds a threshold value in our model. When a cell is divided into two, there is a chance that a newly introduced cell is a cancer cell. In this approach, we assume that a recently divided cell becomes a cancer cell with a probability p. Also, a cancer cell can only be divided into cancer cells.

2.4.3 Using Cascading Failures to analyze robustness of Underlying network to flow re-distribution

Cancerous tumors typically lead to significant reductions in the capacity of blood vessels within cells to transport oxygen throughout tissue, a condition often referred to as hypoxia ([Alt et al., 2017]). This necessitates the natural re-routing of oxygen pathways through other cells in the tissue. However, the failure of one pathway can induce further pathway failures due to reduced capacity, resulting in cascading failures.

Additionally, there is evidence indicating that the stiffness of cancer cells is generally lower than that of normal cells. This phenomenon is observed in certain types of cancer, although exceptions exist; for instance, metastatic pancreatic cancer cells and normal cells exhibit similar stiffness ([**?**]). In contrast, liver and prostate cancer cells are reported to be 1.4-2 times stiffer than normal cells ([**?**]).

We recreate these scenarios using a model of robustness based on resistance to cascading failures.

First, we define a weight re-distribution rule known as the Local Weighted Flow Redistribution Rule (LWFRR)([Wang and Chen, 2008]). In this model, the weight of each edge in the underlying graph is represented as $w_{ij} = (k_i k_j)^\theta$, where k_i denotes the degree of node i and θ is a tunable parameter. This formulation is applicable to many real-world networks and, in our case, indicates that edges with more neighbors have higher edge weights. These weights correspond to diffusion coefficients, implying that pathways surrounded by more oxygen-containing cells have higher diffusion coefficients.

We then select a threshold $T > 1$ and let $T \cdot w_{ij}$ denote the capacity of the edge. This approach assigns higher capacities to edges with higher weights, mirroring real-world situations where edges with higher diffusion coefficients tend to have higher capacities and vice versa.

Once an edge w_{ij} is broken

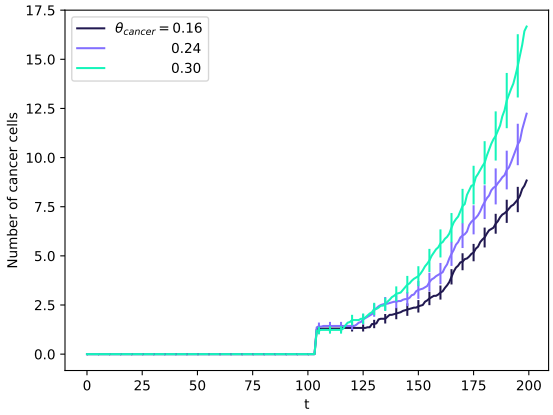

Figure 8: The effect of a variable θ_{cancer} in cancer growth. Simulation results show the number of cancer cells are increased with a larger θ_{cancer} in an identical simulation times.

The increase in a neighbouring edge w_{im} is given by:

$$w_{im} = w_{im} + \frac{w_{ij} \cdot w_{im}}{\sum_a w_{ia} + \sum_b w_{jb}}$$

where a are the edges in the neighborhood of node i and b are the edges in the neighborhood of node j.

We allocate a higher proportion of weight to neighboring edges with greater weights, which effectively corresponds to selecting re-distribution paths with larger capacities within the network.

During the re-distribution process, if an edge exceeds its capacity, it results in overflow and triggers cascading failures. This process continues iteratively until equilibrium is reached within the system.

To assess the robustness of simulated biological networks against cascading failures, we implemented a measure of robustness. Additionally, we configured scenarios to vary the 'stiffness' of cells within the tissue. This was achieved by introducing Gaussian noise, scaled by a constant factor, into the construction of the hexagonal centers for the Voronoi plot. Consequently, this modification produced a more distorted Delaunay triangulation and an altered adjacency matrix.

With a constant noise level, we initially analyzed the robustness of simulated cancer cells compared to healthy cells under cascading failures. For this analysis, we set θ at 1.5 and T at 1.2 for cancer cells, and θ at 2 and T at 1.5 for healthy cells. This reflects that cancer cells possess reduced capacity tolerance (T) and smaller diffusion coefficients. Running 1000 simulations, we tracked the number of iterations required for the network to be completely broken, i.e., all nodes are isolated. This process was repeated for both noisy (stiff) and noise-free (non-stiff) conditions.

3 Results

3.1 Cancer growth around the source node

Figure 8 shows simulation results of oxygen diffusion in a tissue with a oxygen source at the center. It is observed that the number of cancer cells in a given time shows some differences according to a variable θ_{cancer}. To be specific, simulations show more cancer cells with higher θ_{cancer}.

This phenomena could be understood in a following manner. Initially, concentration of nodes other than the source is zero. As a simulation progresses, the oxygen concentration of cells around the source becomes rich and cells are divided. The newly introduced cells can become a cancer cells with a given probability p and the source is soon surrounded by cancer cells. The diffusion across the cancer cells become faster as the variable θ_{cancer} increases. As a result, the oxygen could flow from the center of the system to its boundary very easily. In that case, it is more likely that new cancer cells could be formed relatively far away from the source.

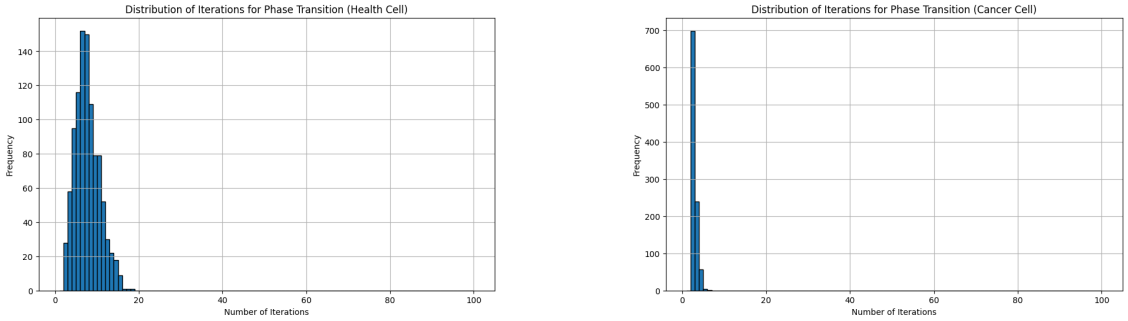

(a) Healthy (b) Cancer

Figure 9: Histogram of the number of iterations needed for network failure over 1000 runs in our simulated cancer and healthy network

Comparison Type	Statistic	P-value
Noisy vs Normal Cell	0.78327	0.433469
Healthy vs Cancer Cell	36.698343	7.761281e-295

Table 1: Rank Sum Test Results for Different Cell Comparisons

3.2 Cascading Failure Robustness Analysis

The results visualized in Figure 9 are fascinating as we note our model correlate well to real life observations of cancer cell behaviour. As expected Tissues with cancer cells show lower levels robustness to cascading failures with usually 0-5 iterations being enough to completely break the system. Higher capacities and diffusion coefficients clearly indicate a wider distribution of values with the mode at around 10 iterations. We also did the same analysis for different levels of Gaussian noise (plot not included for brevity).

Table 1 shows the results of a Non-Parametric Wilcoxon Rank sum test for significant differences. While a reduction in Oxygen transport capacity clearly causes a significant difference between the distributions, merely varying the stiffness keeping all other factors constant does not cause a significant difference. This indicates that in our model while hypoxia definately reduces the robustness of the network, it can not be deduced changes in stiffness alone can cause degradation of the network and thus eventual cell and tissue death.

3.3 Oxygen dependent cell division and Finite Element Method

The vertex model was employed to simulate the dynamics of cancerous and healthy cells within a tissue, focusing on the role of oxygen concentration in cell division. This analysis has been performed at fixed values of oxygen given by the simulation of diffusion. The model incorporates cell mechanics and biophysical properties to capture the behavior of cells in a two-dimensional plane. Healthy cells require a higher threshold of oxygen concentration (0.8) to divide compared to cancer cells (0.1). This difference in oxygen thresholds leads to distinct growth patterns between the two cell populations. On the other hand the Finite Element Method (FEM) simulations focused on modeling the diffusion of oxygen at fixed cell grid. Visualizations of the diffusion process showed the spread of oxygen over time, with lower concentrations in the center and higher towards the edges in a static cellular network using Delaunay triangulations, as expected from the set boundary conditions. Coupling the vertex model with FEM simulations could yield a more comprehensive understanding of tissue dynamics by integrating the detailed spatial distribution of oxygen with the mechanical and proliferative behaviors of cells. The coupled model would allow for a dynamic interaction where oxygen diffusion directly influences cell division and morphology in real-time.

4 Discussion

Our study underscores the complexity of cancer tissue growth and the critical role of oxygen diffusion in influencing cellular behavior. It also study two different populations: normal cell and cancer cell, where the cell cycle time depends on the oxygen concentration.

Oxygen diffusion is a crucial factor in determining cell survival, proliferation, and overall tissue health. The presence of oxygen gradients can lead to differential growth patterns, with cancer cells thriving in oxygen-rich areas. The heterogeneity in diffusion coefficients between normal and cancer cells creates complex diffusion landscapes, affecting nutrient availability and metabolic processes within the tissue.

The model highlights how cancer cells can exploit oxygen availability to proliferate, suggesting that targeting oxygen supply could be a viable therapeutic strategy. By modulating oxygen diffusion, it may be possible to control or limit cancer growth. The probabilistic approach to cancer cell introduction through cell division provides a realistic depiction of tumor heterogeneity and progression.

The concept of cascading failures offers a novel perspective on tissue resilience and vulnerability. Our findings indicate that cancerous tissues are less robust to failures in oxygen transport pathways, leading to potential areas of tissue hypoxia and necrosis. The difference in robustness between cancerous and healthy networks emphasizes the importance of maintaining efficient oxygen transport to support healthy tissue function.

While our model is based solely on simulated data, this process can be replicated on real life data. By obtaining diffusion coefficients from empirical observations and the general spatial structure from real data, cell's could be compared for significant changes in robustness to cascading failures. This can indicate the presence of hypoxia and potentially a malignant tumour. This is merely a hypothesis of course and future work should focus on applying this to real data, preferably with a known ground truth. Further work on the interaction between stiffness and oxygen capacity using network models and its effect on tissue cells in different forms of cancer is also a promising avenue as these two properties could very well be dependant on each other.

Further research is needed to refine these models and apply them to clinical scenarios, enhancing their relevance and applicability in oncology. One of the future goals is to integrate our vertex model with the finite element method (FEM) simulation of the diffusion equation to create a more comprehensive model of tissue dynamics. In the vertex model, when a cell divides, it produces two new cells of the same type, each with half the original cell's oxygen concentration, and involves the creation of four new nodes while removing the old cell's centroid. Separately, we've simulated oxygen diffusion using FEM, utilizing grid points derived from the Delaunay triangulation of the Voronoi diagrams of the cells in the vertex model. By coupling these methods, we aim to start with an initial oxygen concentration, iterate the vertex model to identify any cell divisions, then use the updated points and oxygen concentrations to advance the diffusion simulation using FEM. This iterative process will allow us to simulate how oxygen diffusion throughout the tissue affects the cell cycle, providing valuable insights into tissue dynamics and the progression of diseases such as cancer.

Understanding the interplay between oxygen diffusion and cell mechanics can inform the development of treatments that target the physical and biochemical environment of tumors. Strategies that enhance oxygen delivery or disrupt cancer cell-specific diffusion pathways could improve therapeutic outcomes. Future research should explore the application of these models to empirical data, validating the simulations with real-world measurements of diffusion coefficients and tissue structures. Our study provides a mathematical and physical framework for investigating the dynamics of oxygen diffusion and its impact on cancer tissue growth. The insights gained from this work contribute to a deeper understanding of tumor biology and open avenues for innovative treatment approaches.

5 Acknowledgements

This work is the output of the Complexity72h workshop, held at the Universidad Carlos III de Madrid in Leganés, Spain, 24-28 June 2024. https://www.complexity72h.com

P.G. and N.B. acknowledge grant no. PID2022-141802NB-I00 (BASIC) funded by MCIN/AEI/10.13039/501100011033 and, by 'ERDF A way of making Europe'.

O.R. is supported by the Engineering and Physical Sciences Research Council (EPSRC) Student Excellence Award (SEA) Studentship provided by the United Kingdom Research and Innovation (UKRI) council.

References

K. A. Rejniak. *Systems Biology of Tumor Microenvironment*. Springer International Publishing, 2016. ISBN 9783319420233. doi:10.1007/978-3-319-42023-3. URL http://dx.doi.org/10.1007/978-3-319-42023-3.

S. Alt, P. Ganguly, and G. Salbreux. Vertex models: from cell mechanics to tissue morphogenesis. *Philosophical Transactions of the Royal Society B: Biological Sciences*, 372(1720):20150520, March 2017. ISSN 1471-2970. doi:10.1098/rstb.2015.0520. URL http://dx.doi.org/10.1098/rstb.2015.0520.

J. Metzcar, Y. Wang, R. Heiland, and P. Macklin. A review of cell-based computational modeling in cancer biology. *JCO Clin. Cancer Inform.*, 3(3):1–13, February 2019.

G. Trichas, A. M Smith, N. White, V. Wilkins, T. Watanabe, A. Moore, B. Joyce, J. Sugnaseelan, T. A Rodriguez, D. Kay, R. E Baker, P. K. Maini, and S. Srinivas. Multi-cellular rosettes in the mouse visceral endoderm facilitate the ordered migration of anterior visceral endoderm cells. *PLoS Biol.*, 10(2):e1001256, February 2012.

J. Kursawe, P. A. Brodskiy, J. J. Zartman, R. E. Baker, and A. G. Fletcher. Capabilities and limitations of tissue size control through passive mechanical forces. *PLOS Computational Biology*, 11(12):e1004679, December 2015. ISSN 1553-7358. doi:10.1371/journal.pcbi.1004679. URL http://dx.doi.org/10.1371/journal.pcbi.1004679.

P. Friedl and D. Gilmour. Collective cell migration in morphogenesis, regeneration and cancer. *Nat. Rev. Mol. Cell Biol.*, 10(7):445–457, July 2009.

T. Nagai and H. Honda. A dynamic cell model for the formation of epithelial tissues. *Philosophical Magazine B*, 81(7): 699–719, July 2001. doi:10.1080/13642810108205772. URL https://doi.org/10.1080/13642810108205772.

D. Drasdo. Buckling instabilities of one-layered growing tissues. *Physical Review Letters*, 84(18):4244–4247, May 2000. doi:10.1103/physrevlett.84.4244. URL https://doi.org/10.1103/physrevlett.84.4244.

R. Farhadifar, J.-C. Röper, B. Aigouy, S. Eaton, and F. Jülicher. The influence of cell mechanics, cell-cell interactions, and proliferation on epithelial packing. *Current Biology*, 17(24):2095 – 2104, 2007. ISSN 0960-9822. doi:http://dx.doi.org/10.1016/j.cub.2007.11.049. URL http://www.sciencedirect.com/science/article/pii/S0960982207023342.

S. R. McKeown. Defining normoxia, physoxia and hypoxia in tumours-implications for treatment response. *British Journal of Radiology*, 87(1035):20130676, 2014.

T. Alarcón, H.M. Byrne, and P.K. Maini. A mathematical model of the effects of hypoxia on the cell-cycle of normal and cancer cells. *Journal of Theoretical Biology*, 229(3):395–411, August 2004. ISSN 0022-5193. doi:10.1016/j.jtbi.2004.04.016. URL http://dx.doi.org/10.1016/j.jtbi.2004.04.016.

D. Hanahan and R. A. Weinberg. Hallmarks of cancer: The next generation. *Cell*, 144(5):646–674, 2011.

P. Guerrero, H. M. Byrne, P. K. Maini, and T. Alarcón. From invasion to latency: intracellular noise and cell motility as key controls of the competition between resource-limited cellular populations. *Journal of Mathematical Biology*, 72: 123–156, 2016. doi:10.1007/s00285-015-0883-2.

P. Macklin. When seeing isn't believing: How math can guide our interpretation of measurements and experiments. *Cell Systems*, 5(2):92–94, 2017. doi:10.1016/j.cels.2017.08.005. URL https://pubmed.ncbi.nlm.nih.gov/28837815/.

M. Park, J. Ji, Keeok Haam, T. Han, Seona Lim, Mi-Jung Kang, S. Lim, and H. Ban. Licochalcone a inhibits hypoxia-inducible factor-1 accumulation by suppressing mitochondrial respiration in hypoxic cancer cells. *Biomedicine pharmacotherapy = Biomedecine pharmacotherapie*, 133:111082, 2021. doi:10.1016/j.biopha.2020.111082. URL https://consensus.app/papers/licochalcone-inhibits-accumulation-suppressing-park/a75f76560f195788b888d444bb00be3d/?utm_source=chatgpt.

P. Ebbesen, K. Eckardt, F. Čiampor, and E. Pettersen. Linking measured intercellular oxygen concentration to human cell functions. *Acta Oncologica*, 43:598–600, 2004. doi:10.1080/02841860410020220. URL https://consensus.app/papers/linking-measured-oxygen-concentration-human-cell-ebbesen/3d241b58adb3508082feda8db5d84598/?utm_source=chatgpt.

V. Infantino, A. Santarsiero, P. Convertini, S. Todisco, and V. Iacobazzi. Cancer cell metabolism in hypoxia: Role of hif-1 as key regulator and therapeutic target. *International Journal of Molecular Sciences*, 22, 2021. doi:10.3390/ijms22115703. URL https://consensus.app/papers/cancer-cell-metabolism-hypoxia-role-hif1-regulator-infantino/d8ac3708e3cb5ff9a28266fcdf5f6148/?utm_source=chatgpt.

A. Nagao, Minoru Kobayashi, S. Koyasu, Christalle C.T. Chow, and H. Harada. Hif-1-dependent reprogramming of glucose metabolic pathway of cancer cells and its therapeutic significance. *International Journal of Molecular Sciences*, 20, 2019. doi:10.3390/ijms20020238. URL https://consensus.app/papers/hif1dependent-reprogramming-glucose-metabolic-pathway-nagao/55e6a03011bb5b65b2d8323f53150fb1/?utm_source=chatgpt.

K. Cho, H.-W. Shin, Y.-I. Kim, C. Cho, Y. Chun, T.-Y. Kim, and J.-W. Park. Mad1 mediates hypoxia-induced doxorubicin resistance in colon cancer cells by inhibiting mitochondrial function. *Free radical biology medicine*, 60:201–210, 2013. doi:10.1016/j.freeradbiomed.2013.02.022. URL https://consensus.app/papers/mad1-mediates-hypoxiainduced-resistance-colon-cancer-cho/32bc39b312b75a2bb7d1fac55dfb9136/?utm_source=chatgpt.

A. M. Smith, R. E. Baker, D. Kay, and P. K. Maini. Incorporating chemical signalling factors into cell-based models of growing epithelial tissues. *Journal of Mathematical Biology*, 65:441–463, September 2012.

W.-X. Wang and G. Chen. Universal robustness characteristic of weighted networks against cascading failure. *Phys. Rev. E*, 77:026101, Feb 2008. doi:10.1103/PhysRevE.77.026101. URL `https://link.aps.org/doi/10.1103/PhysRevE.77.026101`.